AIP Journal of Applied Physics

Dislocation-induced fields in piezoelectric AlGaN/GaN bimaterial heterostructures

Xueli Han and Ernie Pan

Citation: J. Appl. Phys. **112**, 103501 (2012); doi: 10.1063/1.4765722
View online: http://dx.doi.org/10.1063/1.4765722
View Table of Contents: http://jap.aip.org/resource/1/JAPIAU/v112/i10
Published by the American Institute of Physics.

Dislocation-induced fields in piezoelectric AlGaN/GaN bimaterial heterostructures

Xueli Han[1,a)] and Ernie Pan[2,b)]
[1]*Department of Mechanics, School of Aerospace, Beijing Institute of Technology, Beijing 100081, China*
[2]*Computer Modeling and Simulation Group, University of Akron, Akron, Ohio 44324-3905, USA*

(Received 29 August 2012; accepted 17 October 2012; published online 19 November 2012)

The fields produced by an arbitrary three-dimensional dislocation loop in general anisotropic piezoelectric bimaterials are analyzed. A line-integral formula is developed for the coupled elastic and electric fields induced by a general dislocation loop in piezoelectric bimaterials, and an analytical solution is also obtained for the fields due to a straight dislocation line segment. As a numerical example, the fields, especially the piezoelectric polarization and polarization charge density, induced by a square dislocation loop in AlGaN/GaN heterostructures are studied. Our numerical results show various interesting features associated with different kinds of dislocations relative to the interface. Particularly, we find that when an edge dislocation is parallel and close to the interface, the dislocation-induced peak charge density on the interface becomes comparable to the two-dimensional electric gas (2DEGs) charge density, thus contributing to the 2DEGs on the AlGaN/GaN interface. © *2012 American Institute of Physics*. [http://dx.doi.org/10.1063/1.4765722]

I. INTRODUCTION

Functional materials, such as piezoelectric/ferroelectric materials, have the coupling effect and energy conversion ability between mechanical and electric fields, providing opportunities for applications as multifunctional devices. These functional materials are commonly utilized in devices in the form of heterostructures or composites. Thus, the interface in these heterostructures or composites would greatly influence the properties and functions of the devices. Recently, the piezoelectric GaN and related heterostructures are the subject of considerable research due to their unique physical properties in certain devices. GaN has a large peak electron velocity, large saturation velocity, high thermal stability, and a large band gap, and thus is very suitable as a channel material for light emission or microwave power amplification. For instance, the AlGaN/GaN-based heterostructure field-effect transistors (HFETs) have the outstanding ability of achieving the two-dimensional electric gas (2DEG) with a high-sheet-carrier concentration close to the interface, and therefore they are attractive candidates as light emission devices for applications at microwave frequencies under high voltage and high-power operation.

Piezoelectric nitride heterostructures are mostly formed by epitaxial growth and thus dislocations are common defects in them. Since a dislocation could play an important role in the mechanical and physical behaviors of the structure, understanding its fundamental behaviors in piezoelectric heterostructures is essential. Previously, the structures and fields of dislocations in some piezoelectric/ferroelectric materials were investigated by electron microscope/holography.[1–6] The dislocation fields in piezoelectric materials were studied mostly in two-dimensional spaces.[7–12] Furthermore, for simplicity, the piezoelectric effect and/or its inverse effect were often neglected when analyzing the dislocation-induced field in piezoelectricity. For instance, the inverse piezoelectric effect was neglected in obtaining the electric field induced by a dislocation[10,13] and the elastic field was not considered in modeling a charged dislocation.[14–18] In reality, however, the dislocation field is fully piezoelectric coupled and dislocations usually form three-dimensional (3D) loops, which prohibits analytical solutions of the relevant problems in most cases.[19–22] Yet, 3D dislocations in piezoelectric materials could show some interesting features and deserve further investigation. For example, the dislocation-induced piezoelectric polarization and polarization charges, the electron scattering effect by dislocations, and the direct dislocation influence near the interface of the heterostructures are all important for the related device design.

In the present work, we will analytically study the interaction between a dislocation loop and an interface in a piezoelectric bimaterial. Based on the "point-force" Green's function in a piezoelectric bimaterial, we first derive a line integral expression for the fields induced by a 3D dislocation loop in a general anisotropic piezoelectric bimaterial system. We then obtain an analytical solution for the fields due to a straight line dislocation segment. With this analytical solution, we can calculate the fields produced by an arbitrary 3D dislocation loop with great efficiency and accuracy, and study its interaction with the interface in a piezoelectric bimaterial structure. As an example, the fields induced by a square dislocation loop in AlGaN/GaN piezoelectric heterostructures are calculated, with the piezoelectric polarization and polarization charges being shown in details. Our results show various interesting features associated with different dislocation types and material poling directions.

II. MODEL AND METHOD

The problem of interest consists of a dislocation loop in two joined half-spaces with dissimilar piezoelectric material properties. Figure 1 illustrates a square dislocation loop in

a)E-mail address: hanxl@bit.edu.cn.
b)E-mail address: pan2@uakron.edu.

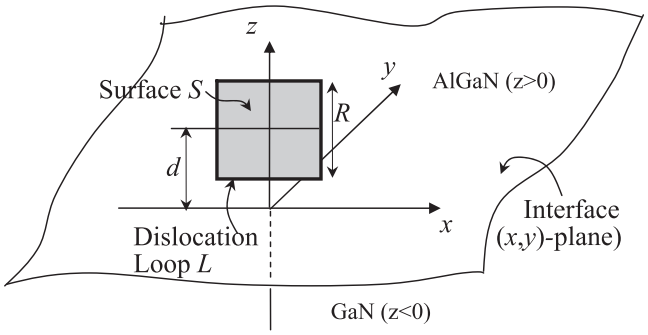

FIG. 1. Schematic of a square dislocation loop in AlGaN/GaN bimaterials.

the AlGaN/GaN bimaterial. We will derive the fields induced by a dislocation loop in such a bimaterial system.

The linear constitutive relations for the coupled piezoelectric media can be written as

$$\begin{cases} \sigma_{ij} = c_{ijlm}\gamma_{lm} - e_{kij}E_k \\ D_i = e_{ijk}\gamma_{jk} + \varepsilon_{ij}E_j \end{cases}, \tag{1a}$$

where c_{ijlm}, e_{ijk}, and ε_{ij} are the elastic, piezoelectric, and dielectric coefficients, respectively; σ_{ij} and D_i are the stress and electric displacement; γ_{ij} and E_i are the strain and electric field. Equation (1a) can be written in a compact form[23,24]

$$\sigma_{iJ} = C_{iJKl}\gamma_{Kl}, \tag{1b}$$

with a repeated lowercase (uppercase) index taking the summation from 1 to 3 (4), and $\sigma_{iJ}, C_{iJKl}, and\, \gamma_{Kl}$ being the extended stresses, elastic constants, and strains, respectively.

The (extended) displacement field produced by a dislocation loop can be expressed as[25]

$$u_M(\mathbf{y}) = \int_S C_{iJKl}(\mathbf{x})G_{KM,x_l}(\mathbf{y};\mathbf{x})b_J(\mathbf{x})n_i(\mathbf{x})dS(\mathbf{x}), \tag{2}$$

with S being the dislocation surface across which the discontinuity of the displacement and electric potential is described by the extended Burgers vector[7,23] $\mathbf{b} = [b_1, b_2, b_3, \Delta\phi]^{\mathrm{T}}$. Also in Eq. (2), $G_{KM}(\mathbf{y};\mathbf{x})$ are the extended Green's functions in the corresponding media,[26] i.e., the K-th extended displacement component at the field point $\mathbf{x}$ due to the M-th extended unit "point force" component at the source point $\mathbf{y}$; a subscript comma denotes the partial differentiation with respect to the coordinates, i.e., $G_{KM,x_l} = \partial G_{KM}/\partial x_l$. The extended Green's functions and their derivatives in piezoelectric bimaterials are given in Appendix.

In piezoelectric materials, the strain field can induce a piezoelectric polarization field $\mathbf{P}^{Pz}$ as

$$P_i^{Pz} = e_{ijk}\gamma_{jk} = e_{ijk}u_{j,k}. \tag{3}$$

Furthermore, the gradient of $\mathbf{P}^{Pz}$ can induce a piezoelectric polarization charge, with the volume charge density ρ^{Pz} being

$$\rho^{Pz} = \nabla \cdot \mathbf{P}^{Pz} = e_{ijk}u_{j,ki}. \tag{4}$$

It is also noticed that a jump in $\mathbf{P}^{Pz}$ across the interface of the bimaterial can induce piezoelectric polarization charges on the interface, with the surface charge density σ^{Pz} being

$$\sigma^{Pz} = [P_3^{Pz}] = [e_{3jk}u_{j,k}], \tag{5}$$

where $[f]$ denotes the discontinuity across the interface.

It can be seen from Eqs. (3)–(5) that $u_{j,k}$ and $u_{j,ki}$ are both needed in order to obtain $\mathbf{P}^{Pz}$, σ^{Pz}, and ρ^{Pz}. Thus, we will first derive the expressions for the extended displacement and its (first and second) derivatives produced by a dislocation loop in piezoelectric bimaterials. We point out that the second derivative of the displacements due to dislocations has never been reported in any existing literature and that it is the first time that its connection to the charge density is presented in this article. After that, the strain-induced piezoelectric polarization and polarization charges will be evaluated using Eqs. (3)–(5).

When a dislocation loop lies on a plane where the material properties are constants or piecewise constants on the dislocation loop surface S, the extended displacement field and its derivatives can be expressed as the surface integrals below

$$u_M(\mathbf{y}) = C_{iJKl}b_J n_i \int_S G_{KM,x_l}(\mathbf{y};\mathbf{x})dS(\mathbf{x}), \tag{6a}$$

$$u_{M,p\ldots}(\mathbf{y}) = C_{iJKl}b_J n_i \int_S G_{KM,x_l y_{p\ldots}}(\mathbf{y};\mathbf{x})dS(\mathbf{x}). \tag{6b}$$

We will now convert these surface integrals into the simple line integrals. In order to do so, we will first need to analyze the involved Green's functions in Eq. (6).

The Green's functions in bimaterials can be separated into two parts: $\mathbf{G}(\mathbf{y};\mathbf{x}) = \mathbf{G}^{\infty}(\mathbf{y};\mathbf{x}) + \mathbf{G}^{Image}(\mathbf{y};\mathbf{x})$, where $\mathbf{G}^{\infty}(\mathbf{y};\mathbf{x})$ corresponds to the full-space part and $\mathbf{G}^{Image}(\mathbf{y};\mathbf{x})$ is called the image or complementary term which is associated with the bimaterial interface. Correspondingly, the derivatives of the Green's function can be separated into a full-space and an image part. Thus, the integral $\int_S G_{KM,x_l\ldots}(\mathbf{y};\mathbf{x})dS(\mathbf{x})$ can be also separated into two parts as

$$\int_S G_{KM,x_l\ldots}(\mathbf{y};\mathbf{x})dS(\mathbf{x}) = \int_S G^{\infty}_{KM,x_l\ldots}(\mathbf{y};\mathbf{x})dS(\mathbf{x}) + \int_S G^{Image}_{KM,x_l\ldots}(\mathbf{y};\mathbf{x})dS(\mathbf{x}). \tag{7}$$

The first part of the surface integral contains the derivatives of the full-space Green's function. For this part, a line integral expression (along the loop L of the dislocation) for the induced field is given as[25]

$$u_{M,p\ldots}(\mathbf{y}) = -\varepsilon_{iph}C_{iJKl}b_M \int_L G^{\infty}_{KM,x_l\ldots}(\mathbf{y};\mathbf{x})\nu_h(\mathbf{x})dL(\mathbf{x}), \tag{8}$$

which can be calculated by a numerical integration method. In Eq. (8), ε_{iph} is the permutation tensor and $\boldsymbol{\nu}$ the unit tangential vector along the positive loop direction.

As for the image part, by substituting the solution $G^{Image}_{KM,x_l\ldots}(\mathbf{y};\mathbf{x})$ in Appendix into the integral in Eq. (7) and using the unit "point force" solution at $y_3 > 0$, we have, for the field at $y_3 > 0$,

$$\int_S \mathbf{G}(\mathbf{y};\mathbf{x})^{Image}_{,x_l\ldots y_p} \mathrm{d}S(\mathbf{x}) = \begin{cases} \dfrac{1}{2\pi^2}\displaystyle\int_0^\pi \bar{\mathbf{A}}^{(1)}\left[\int_S (\mathbf{G}_u^{(1)})_{,x_l\ldots y_p}\mathrm{d}S(\mathbf{x})\right](\mathbf{A}^{(1)})^T\mathrm{d}\theta, & \text{when } x_3>0 \\ \dfrac{1}{2\pi^2}\displaystyle\int_0^\pi \mathbf{A}^{(2)}\left[\int_S (\mathbf{G}_u^{(2)})_{,x_l\ldots y_p}\mathrm{d}S(\mathbf{x})\right](\mathbf{A}^{(1)})^T\mathrm{d}\theta, & \text{when } x_3<0 \end{cases}, \tag{9}$$

with

$$\begin{cases} \displaystyle\int_S (\mathbf{G}_u^{(1)})_{IJ,x_l}\mathrm{d}S(\mathbf{x}) = (\mathbf{G}_1)_{IJ}h_l(\theta,\bar{p}_I^{(1)})\int_S \frac{\mathrm{d}S(\mathbf{x})}{[-\mathbf{h}(\theta,\bar{p}_I^{(1)})\cdot\mathbf{x}+\mathbf{h}(\theta,p_J^{(1)})\cdot\mathbf{y}]^2} \\ \displaystyle\int_S (\mathbf{G}_u^{(2)})_{IJ,x_l}\mathrm{d}S(\mathbf{x}) = (\mathbf{G}_2)_{IJ}h_l(\theta,p_I^{(2)})\int_S \frac{\mathrm{d}S(\boldsymbol{x})}{[-\mathbf{h}(\theta,p_I^{(2)})\cdot\mathbf{x}+\mathbf{h}(\theta,p_J^{(1)})\cdot\mathbf{y}]^2} \end{cases}, \tag{10a}$$

$$\begin{cases} \displaystyle\int_S (\mathbf{G}_u^{(1)})_{IJ,x_ly_p}\mathrm{d}S(\mathbf{x}) = -2(\mathbf{G}_1)_{IJ}h_l(\theta,\bar{p}_I^{(1)})h_p(\theta,p_J^{(1)})\int_S \frac{\mathrm{d}S(\mathbf{x})}{[-\mathbf{h}(\theta,\bar{p}_I^{(1)})\cdot\mathbf{x}+\mathbf{h}(\theta,p_J^{(1)})\cdot\mathbf{y}]^3} \\ \displaystyle\int_S (\mathbf{G}_u^{(2)})_{IJ,x_ly_p}\mathrm{d}S(\mathbf{x}) = -2(\mathbf{G}_2)_{IJ}h_l(\theta,p_I^{(2)})h_p(\theta,p_J^{(1)})\int_S \frac{\mathrm{d}S(\mathbf{x})}{[-\mathbf{h}(\theta,p_I^{(2)})\cdot\mathbf{x}+\mathbf{h}(\theta,p_J^{(1)})\cdot\mathbf{y}]^3} \end{cases}, \tag{10b}$$

$$\begin{cases} \displaystyle\int_S (\mathbf{G}_u^{(1)})_{IJ,x_ly_py_q}\mathrm{d}S(\mathbf{x}) = 6(\mathbf{G}_1)_{IJ}h_l(\theta,\bar{p}_I^{(1)})h_p(\theta,p_J^{(1)})h_q(\theta,p_J^{(1)})\int_S \frac{\mathrm{d}S(\mathbf{x})}{[-\mathbf{h}(\theta,\bar{p}_I^{(1)})\cdot\mathbf{x}+\mathbf{h}(\theta,p_J^{(1)})\cdot\mathbf{y}]^4} \\ \displaystyle\int_S (\mathbf{G}_u^{(2)})_{IJ,x_ly_py_q}\mathrm{d}S(\mathbf{x}) = 6(\mathbf{G}_2)_{IJ}h_l(\theta,p_I^{(2)})h_p(\theta,p_J^{(1)})h_q(\theta,p_J^{(1)})\int_S \frac{\mathrm{d}S(\boldsymbol{x})}{[-\mathbf{h}(\theta,p_I^{(2)})\cdot\mathbf{x}+\mathbf{h}(\theta,p_J^{(1)})\cdot\mathbf{y}]^4} \end{cases}. \tag{10c}$$

In Eq. (10), $\mathbf{h}(\theta,p)$, $(\mathbf{G}_u^{(1)})_{IJ}$, $(\mathbf{G}_u^{(2)})_{IJ}$, and their derivatives can be found in Appendix. For the field at $y_3<0$, similar results can be obtained.

It is obvious from Eq. (10) that the key issue is to treat the following type of surface integral (over the dislocation surface):

$$F_n(\mathbf{y},\theta,p_1,p_2) = \int_S \frac{\mathrm{d}S(\mathbf{x})}{[-\mathbf{h}(\theta,p_1)\cdot\mathbf{x}+\mathbf{h}(\theta,p_2)\cdot\mathbf{y}]^n} \quad n=2,3,4, \tag{11}$$

where p_1 and p_2 can be assigned to different eigenvalues according to the corresponding expressions of the Green's functions involved.

While exact integral of Eq. (11) over a dislocation loop surface cannot be found in general, we will convert the involved surface integral to a simple line integral. In order to do so, we first transform the global coordinate system (O:x_1,x_2,x_3) to a local one ($\mathbf{x}^0$:ξ_1,ξ_2,ξ_3) by $[\mathbf{x}-\mathbf{x}^0]=[\mathbf{D}][\boldsymbol{\xi}]$, with the ($\xi_1$,$\xi_2$)-plane being on the dislocation surface plane and with $\mathbf{x}^0$ being the origin of the local coordinates. Then, the integration in Eq. (11) becomes

$$F_n(\mathbf{y},\theta,p) = \int_S \frac{\mathrm{d}\xi_1\mathrm{d}\xi_2}{[f_1(\mathbf{y},\theta)\xi_1+f_2(\mathbf{y},\theta)\xi_2+f_3(\mathbf{y},\theta)]^n}, \quad n=2,3,4, \tag{12}$$

with $f_\alpha(\mathbf{y},\theta)=-D_{k\alpha}h_k(\theta,p_1), \alpha=1,2$ and $f_3(\mathbf{y},\theta)=y_kh_k(\theta,p_2)-x_k^0h_k(\theta,p_1)$.

By introducing

$$L_n(\xi_1,\xi_2) = \int_{-\infty}^{\xi_2}\frac{\mathrm{d}\xi_2}{(f_1\xi_1+f_2\xi_2+f_3)^n} = -\frac{1}{(n-1)f_2}\frac{1}{(f_1\xi_1+f_2\xi_2+f_3)^{n-1}}, \quad n=2,3,4, \tag{13}$$

we arrive at

$$F_n = \int_S \frac{\partial L_n(\xi_1,\xi_2)}{\partial\xi_2}\mathrm{d}\xi_1\mathrm{d}\xi_2 = \int_L L_n(\xi_1,\xi_2)\mathrm{d}\xi_1 = \frac{-1}{(n-1)f_2}\int_L \frac{\mathrm{d}\xi_1}{(f_1\xi_1+f_2\xi_2+f_3)^{n-1}}, \quad n=2,3,4. \tag{14}$$

Thus, the surface integral over the dislocation plane is reduced to the line integral along the dislocation loop line L.

Since an arbitrarily shaped dislocation loop can be approximated as a summation of a number of connected straight dislocation segments, we will derive the solution of a straight dislocation segment. For a straight line in the local (ξ_1, ξ_2)-plane, it can be described by

$$\boldsymbol{\xi}(t) = (1-t)\mathbf{P}_1 + t\mathbf{P}_2, \quad 0\le t\le 1, \tag{15}$$

with $\mathbf{P}_1$, $\mathbf{P}_2$ being the position vectors of the start and end points of the straight line segment. Then, the integral

TABLE I. Material properties: Material properties of GaN, AlN, and AlGaN (transverse isotropy with poling along x_3-axis).

	C_{11}	C_{12}	C_{13}	C_{33}	C_{44}	a_0 (Å)
GaN	367	135	103	405	95	3.189
AlN	396	137	108	373	116	3.112
AlGaN	381.5	136	105.5	389	105.5	3.1505
	e_{31}	e_{33}	e_{15}	ε_{11}	ε_{33}	P^{Sp}
GaN	−0.36	1.0	−0.3	9.5	10.4	−0.029
AlN	−0.58	1.55	−0.48	9.0	10.5	−0.081
AlGaN	−0.47	1.275	−0.39	9.25	10.55	−0.055

Elastic constants C_{ij} are in GPa, piezoelectric constants e_{ij} and spontaneous polarization P^{Sp} in C/m^2, and the dielectric constants ε_{ij} are relative to $\varepsilon_0 = 8.8541878 \times 10^{-12}$ F/m.

in Eq. (14) can be carried out exactly, with the following expressions:

$$F_2^{Segment} = -\frac{1}{f_2}\frac{P_{21}-P_{11}}{f_1(P_{21}-P_{11})+f_2(P_{22}-P_{12})} \times \mathrm{In}\frac{f_1P_{21}+f_2P_{22}+f_3}{f_1P_{11}+f_2P_{12}+f_3}, \tag{16a}$$

$$F_3^{Segment} = \frac{1}{2f_2}\frac{P_{21}-P_{11}}{f_1(P_{21}-P_{11})+f_2(P_{22}-P_{12})} \times \left(\frac{1}{f_1P_{21}+f_2P_{22}+f_3} - \frac{1}{f_1P_{11}+f_2P_{12}+f_3}\right), \tag{16b}$$

$$F_4^{Segment} = \frac{1}{6f_2}\frac{P_{21}-P_{11}}{f_1(P_{21}-P_{11})+f_2(P_{22}-P_{12})} \times \left[\frac{1}{(f_1P_{21}+f_2P_{22}+f_3)^2} - \frac{1}{(f_1P_{11}+f_2P_{12}+f_3)^2}\right]. \tag{16c}$$

III. NUMERICAL EXAMPLES AND RESULTS

We consider a dislocation loop in AlGaN/GaN bimaterials, with AlGaN having 50% Al and 50% Ga. AlN, GaN, and AlGaN are transversely isotropic (or hexagonal) materials with their poling direction along z-axis (i.e., x_3-axis). The material properties of AlN and GaN are adopted from literature,[27,28] and those of AlGaN are calculated by a linear interpolation between the material properties of AlN and GaN, with the results being listed in Table I. As an example, the dislocation loop is assumed to be a square on the x-z plane (i.e., x_1-x_3 plane), with the side length of the loop being R and the distance of loop center to the interface being d, see Fig. 1.

For a dislocation along ⟨100⟩, the piezoelectric polarization vector $\mathbf{P}^{Pz}$ and the contour of its magnitude $|\mathbf{P}^{Pz}|$ on different planes are shown in Fig. 2. The induced volume charge density field ρ^{Pz} is shown in Fig. 3, and the surface charge density field σ^{Pz} on the interface in Fig. 4. From these figures, we observe the following features:

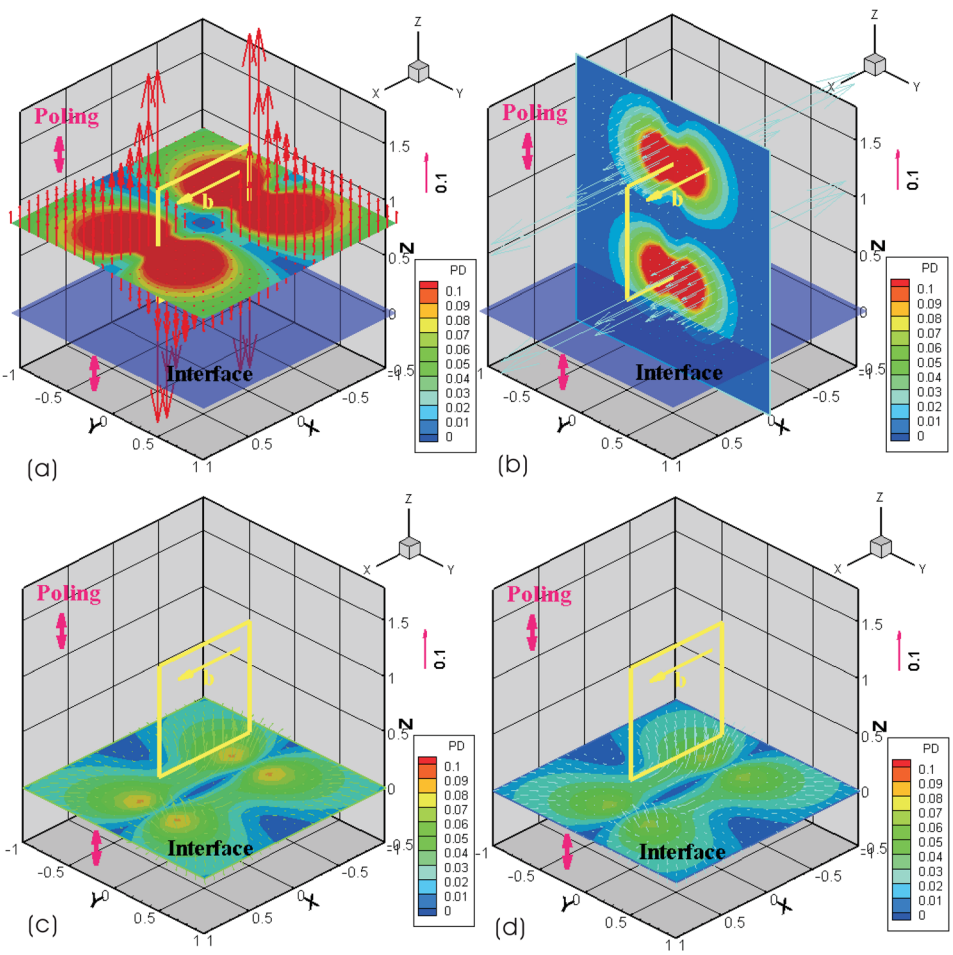

FIG. 2. Dislocation-induced piezoelectric polarization vector P^{Pz} and contour of $|P^{Pz}|$: (a) on plane $z=d$; (b) on plane $x=0$; (c) on plane $z=0+$; (d) on plane $z=0-$. The dislocation is a square loop on the plane (010) with Burgers vector $\mathbf{b}=b[100]$ and $d/R=0.8$. The coordinates are normalized by the side length R of the square. P^{Pz} and $|P^{Pz}|$ are in the unit C/m^2 and are normalized by b/R.

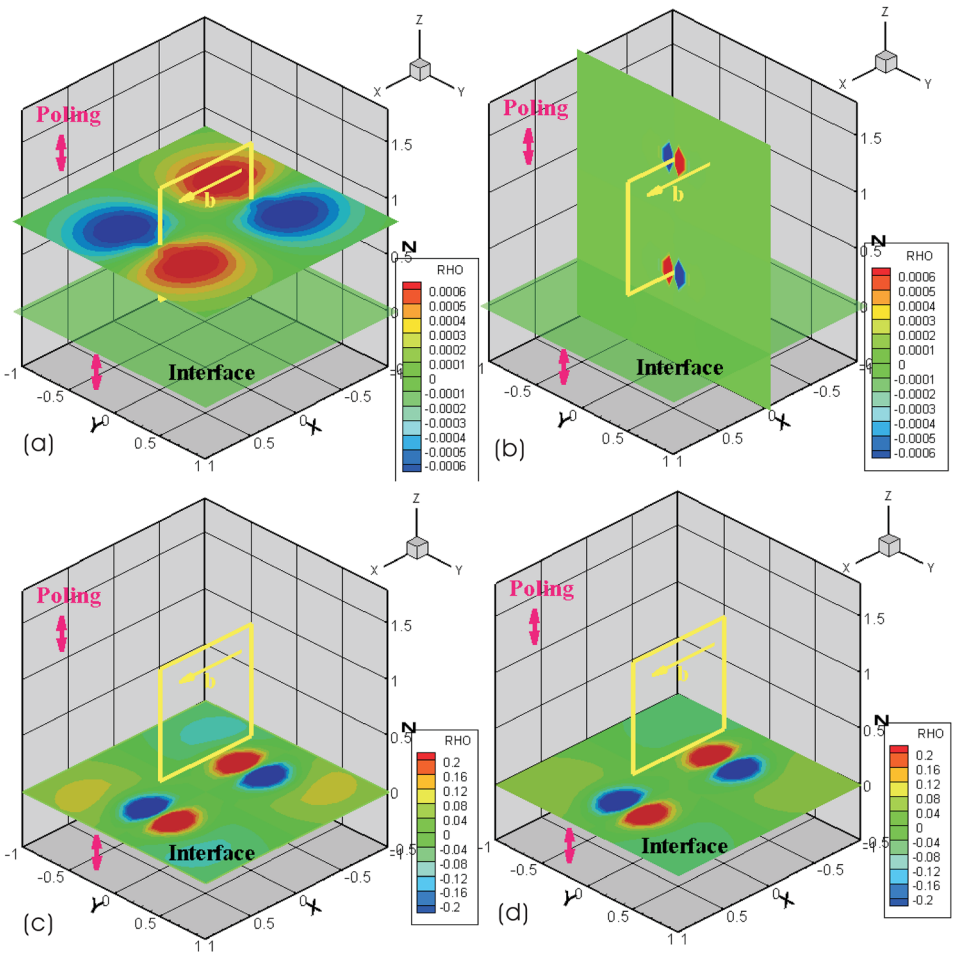

FIG. 3. The charge density ρ^{Pz} induced by the square dislocation with Burgers vector $\mathbf{b} = b[100]$: (a) on plane $z = d$; (b) on plane $x = 0$; (c) on plane $z = 0+$; (d) on plane $z = 0-$. ρ^{Pz} is in the unit of C/m^3 and is normalized by b/R^2.

(a) For an edge dislocation line along the poling direction, the polarization field $\mathbf{P}^{Pz}$ is along the dislocation line (Fig. 2(a)); however, it switches its orientation on the two sides of the dislocation plane (Fig. 2(a)), and its divergence leads to the formation of the dipole-like charge density ρ^{Pz} along the dislocation line (Fig. 3(a)). This result is consistent with that for an infinite dislocation.[10]

(b) When the edge dislocation line is normal and close to the interface, the induced $\mathbf{P}^{Pz}$ on the interface has its major component perpendicular to the interface (Figs. 2(c) and 2(d)). Although $|\mathbf{P}^{Pz}|$ is not large, it has a large divergence which leads to the formation of large dipole-like charges ρ^{Pz} on the interface directly below the dislocation line (Figs. 3(c) and 3(d)). This result also confirms the judgment that edge dislocations that are close and normal to a surface (interface) would give rise to an effective surface (interface) charge.[10] It is noted that on the two sides of the interface, the polarization field $\mathbf{P}^{Pz}$ is similar but with different values (Figs. 2(c) and 2(d)), which can further induce a dipole-like surface charge density field σ^{Pz} on the interface (Fig. 4).

(c) For a screw dislocation perpendicular to the poling direction, the induced $\mathbf{P}^{Pz}$ is along the dislocation line (the same direction of the Burgers vector) (Fig. 2(b)) but opposite on both sides of the $y = 0$ plane (which is also the dislocation plane) (Fig. 2(b)). Its divergence leads to the formation of the dipole-like charge density ρ^{Pz} along the dislocation line (Fig. 3(b)). However, this charge density is much smaller than that induced by an edge dislocation along the poling direction (Fig. 3(a)),

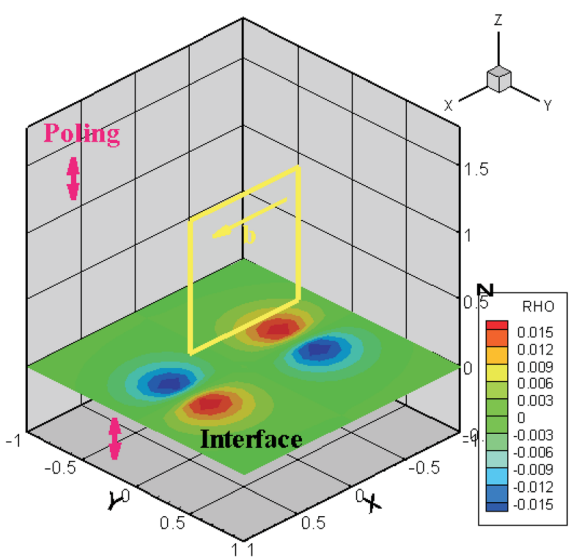

FIG. 4. The surface charge density field σ^{Pz} on the interface $z = 0$ induced by the square dislocation with Burgers vector $\mathbf{b} = b[100]$. σ^{P} is in the unit of C/m^2 and is normalized by b/R.

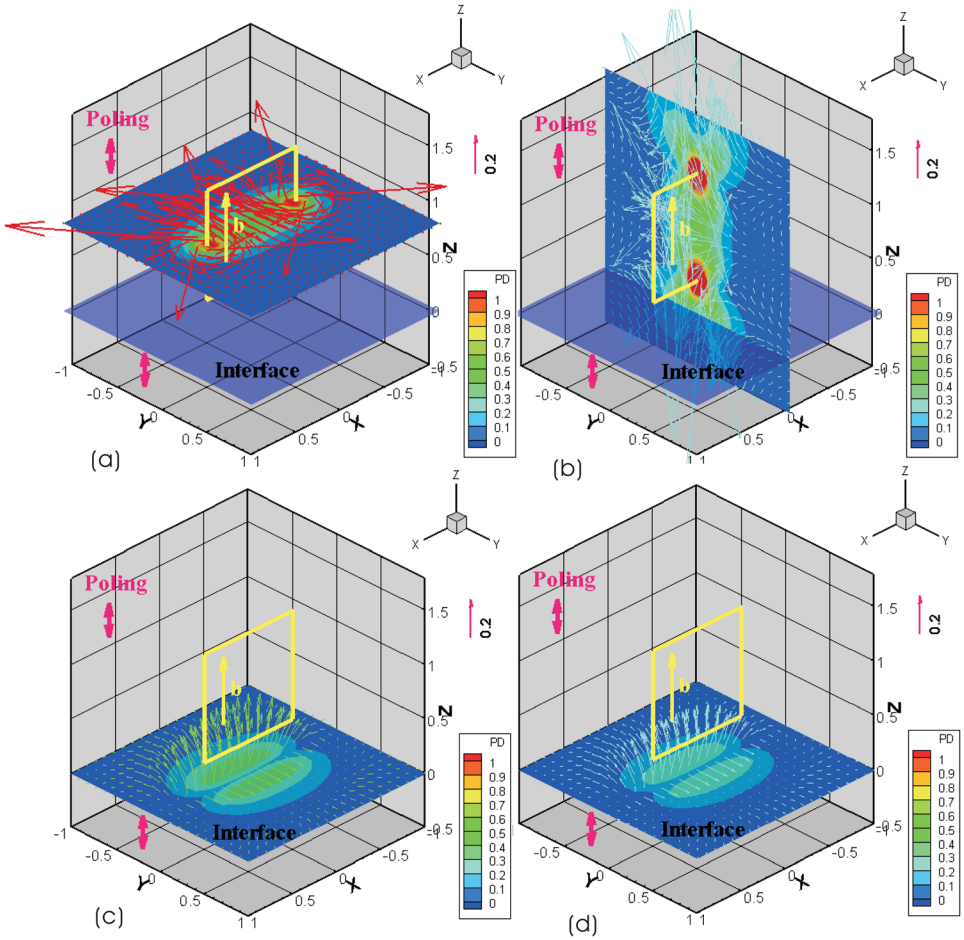

FIG. 5. Dislocation-induced piezoelectric polarization vector P^{Pz} and contour of $|P^{Pz}|$: (a) on plane $z=d$; (b) on plane $x=0$; (c) on plane $z=0+$; (d) on plane $z=0-$. The dislocation is a square loop on the plane (010) with Burgers vector $\mathbf{b}=b[001]$ and $d/R=0.8$. The coordinates are normalized by the side length R of the square. P^{Pz} and $|P^{Pz}|$ are in the unit C/m^2 and are normalized by b/R.

and thus its influence on the interface behavior could be weak (as compared to the effect on the interface by the corresponding edge dislocation).

For a dislocation along ⟨001⟩, the piezoelectric polarization vector $\mathbf{P}^{Pz}$ and contour of $|\mathbf{P}^{Pz}|$ on different planes are shown in Fig. 5. The induced volume charge density field ρ^{Pz} is shown in Fig. 6 and surface charge density field σ^{Pz} on the interface in Fig. 7. The following features can be observed from these figures:

(a) For a screw dislocation along the poling direction, the polarization field $\mathbf{P}^{P}$ is perpendicular to the dislocation line (Fig. 5(a)). It is around the dislocation line and is divergence-free; therefore, there is no polarization-induced charge ρ^{Pz} near the dislocation line (see Fig. 6(a), the charges on the plane are due to the edge dislocations). This result is again consistent with that for an infinite dislocation by Shi *et al.*[10] Thus, its influence on the electric field at the interface would be weak.

(b) For an edge dislocation line perpendicular to the poling direction, the polarization field $\mathbf{P}^{Pz}$ is orthogonal to and around the dislocation line (Fig. 5(b)). Its divergence leads to the formation of octagon-foil pattern of the charge density ρ^{Pz} along the dislocation line (Fig. 6(b)).

(c) When the edge dislocation line is parallel and close to the interface, the induced $\mathbf{P}^{Pz}$ on both sides of the interface has its major component normal to the interface (Figs. 5(c) and 5(d)). Its divergence leads to the formation of the dipole-like charge density ρ^{Pz} on the interface (Figs. 6(c) and 6(d)). It is also observed from Figs. 5(c) and 5(d) that on two sides of the interface, $\mathbf{P}^{Pz}$ is similar but with different values. Thus, this difference of $\mathbf{P}^{Pz}$ on both sides of the interface can further induce the dipole-like surface charge density field σ^{Pz} on the interface (Fig. 7).

In summary, for a dislocation loop in a piezoelectric bimaterial, it will induce piezoelectric polarization around the dislocation line due to the large strain field and elasto-electric coupling effect. For a screw dislocation, the polarization field is (or nearly) divergence free, so it will induce no (or weak) polarization charges and will not disturb the 2DEGs on the interface. On the other hand, the polarization field induced by an edge dislocation has a divergence and this will induce polarization charges around the dislocation line. For an edge dislocation with dislocation line perpendicular to the interface, it will induce polarization charges on the interface directly below the dislocation line (Figs. 3(c), 3(d), 4). For an edge dislocation with dislocation line parallel to the interface, it will induce polarization charges on the interface (Figs. 6(c), 6(d), 7). However, the charge due to a dislocation parallel to the interface (latter case) is much larger than that due to the one normal to the interface (former case). Nevertheless, these dislocation-induced charges will disturb the 2DEGs on the AlGaN/GaN interface.

In order to estimate the dislocation-induced charge effect on the 2DEGs, we further calculate the interface charges density σ^{Pz} for an edge dislocation parallel to the

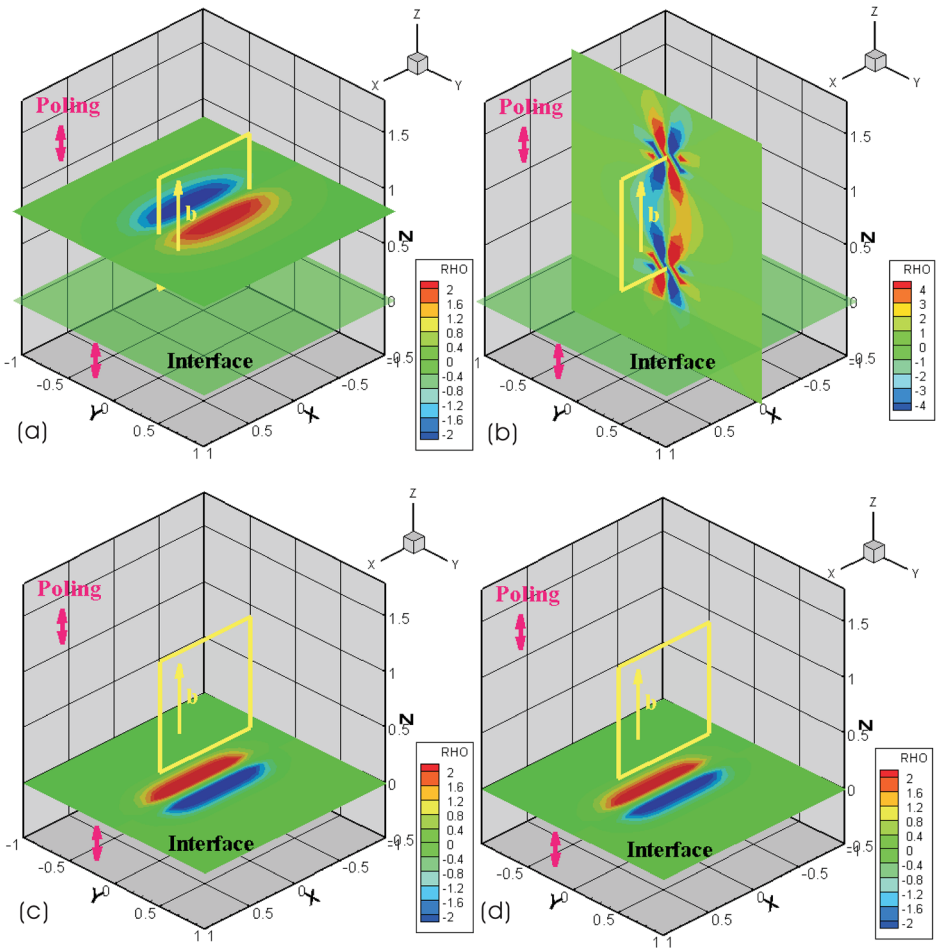

FIG. 6. The charge density ρ^{Pz} induced by the square dislocation with Burgers vector $\mathbf{b} = b[001]$: (a) on plane $z = d$; (b) on plane $x = 0$; (c) on plane $z = 0+$; (d) on plane $z = 0-$. ρ^{Pz} is in the unit of C/m^3 and is normalized by b/R^2.

interface with varying distances to the interface. In this example, the loop is still a square but with a large side length $R = 100a$, so that the main influence to the interface comes from the bottom dislocation line close to the interface (a being the lattice constant). The square is perpendicular to the interface with the loop plane normal along (010), and Burgers vector $\mathbf{b} = b[001]$. The dislocation-induced charge density σ^{Pz} on the interface along y-axis is shown in Fig. 8 for different dislocation distances $h = d - R/2$ to the interface. The peak value of σ^{Pz} is about 0.032 C/m^2 when the dislocation is close to the interface with $h/a = 1$. Figure 9 shows the result for the corresponding case with $\mathbf{b} = b[010]$. Compared to Fig. 8, it is observed that the dislocation-induced interface

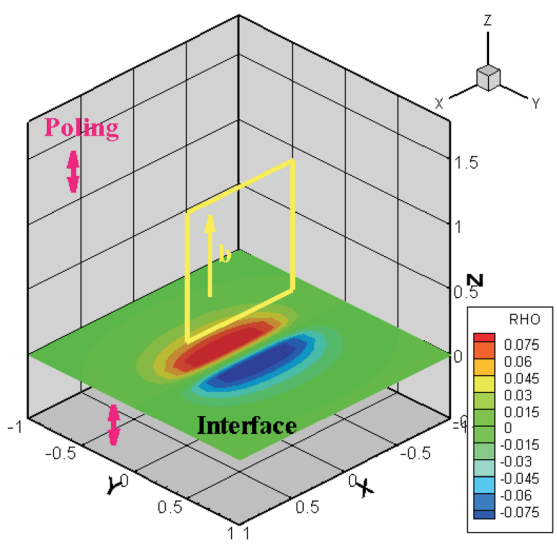

FIG. 7. The surface charge density σ^{Pz} on the interface $z = 0$ induced by the square dislocation with Burgers vector $\mathbf{b} = b[001]$. σ^{Pz} is in the unit of C/m^2 and is normalized by b/R.

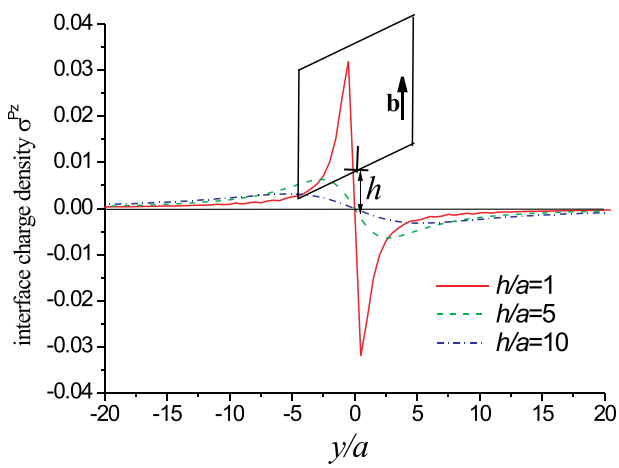

FIG. 8. Dislocation-induced surface charge density σ^{Pz} along y-axis on the interface $z = 0$ for different dislocation distances $h = d - R/2$ to the interface. The dislocation is a square loop with side length $R/a = 100$ on the plane (010), Burgers vector $\mathbf{b} = b[001]$ and $b = a$. The coordinates are normalized by the lattice constant a and σ^{Pz} is in the unit of C/m^2.

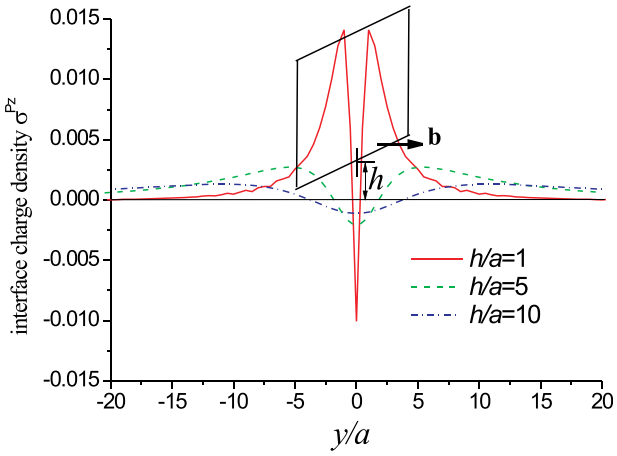

FIG. 9. Dislocation induced surface charge density σ^{Pz} along y-axis on the interface $z=0$ for different dislocation distances $h=d-R/2$ to the interface. The dislocation is a square loop with side length $R/a=100$ on the plane (010), Burgers vector $\mathbf{b}=b[010]$ and $b=a$. The coordinates are normalized by the lattice constant a and σ^{Pz} is in the unit of C/m^2.

charge density σ^{Pz} by $\mathbf{b}=b[010]$ is smaller than that by $\mathbf{b}=b[001]$, and that the peak value of σ^{Pz} is about 0.014 C/m^2 when the dislocation is close to the interface with $h/a=1$ (compared to 0.032 C/m^2 when $\mathbf{b}=b[001]$). With increasing h, the peak value σ^{Pz} decreases very fast.

The 2DEGs on the AlGaN/GaN interface mainly come from the following two parts: the piezoelectric polarization $\mathbf{P}^{Pm}$ due to the lattice mismatch strain at the interface, and the change of spontaneous polarization $\mathbf{P}^{Sp}$ at the interface. The piezoelectric polarization $\mathbf{P}^{Pm}$ due to the lattice strain along the c axis (the poling axis) can be determined by[28,29]

$$P_3^{Pm} = e_{3jk}\gamma_{jk} = 2\frac{a-a_0}{a_0}\left(e_{31} - e_{33}\frac{C_{13}}{C_{33}}\right), \qquad (17)$$

with a_0 being the lattice constant of GaN, and all other quantities corresponding to those of AlGaN. Using the material constants in Table I, we find that P_3^{Pm} in AlGaN (in unrelaxed state) is -0.0199 C/m^2, with an induced surface charge density $\sigma^{Pm} = [P_3^{Pm}] = -0.0199$ C/m^2. The change in spontaneous polarization $\mathbf{P}^{Sp}$ at the interface can also induce a surface charge density as $\sigma^{Sp} = [P_3^{Sp}] = -0.026$ C/m^2. Thus, the sheet charge density on the interface will be around $\sigma^{2\mathrm{DEGs}} = \sigma^{Pm} + \sigma^{Sp} = -0.046$ C/m^2. Since the mismatch strain on AlGaN might be partially relaxed, the sheet charge density $\sigma^{2\mathrm{DEGs}}$ would be around -0.046 C/m^2 to -0.026 C/m^2. We have showed that for an edge dislocation parallel and close to the interface, the dislocation-induced peak charge density σ^{Pz} near the interface could be around 0.032 C/m^2, which is comparable to $\sigma^{2\mathrm{DEGs}} = -0.046$ C/m^2. In other words, the dislocation-induced charges would contribute to and influence the 2DEGs on the AlGaN interface.

IV. CONCLUSION AND DISCUSSION

A full electric-elastic coupled model and the corresponding solution method are presented to evaluate the fields produced by an arbitrary 3D dislocation loop in general anisotropic piezoelectric bimaterials. A line-integral expression along the dislocation loop is derived for the coupled elastic and electric fields, and an analytical solution is obtained for the fields due to a straight dislocation line segment. The fields, especially the piezoelectric polarization and polarization charges, due to a square dislocation loop in AlGaN/GaN heterostructures are studied in detail. Our numerical results show various different and interesting features associated with different kinds of dislocations. The piezoelectric polarization field induced by an edge dislocation is not divergent free, and thus it can induce electric charges near the dislocation. When an edge dislocation is close to the interface, it will also induce polarization charges on the interface. Furthermore, the induced peak charge density at the interface could be comparable to the 2DEGs charge density, and thus the dislocation will influence the 2DEGs on the interface.

In the present model, we have assumed that the materials are insulator without free charges. For n- or p-doped semiconductors, external charged impurities are often accumulated on the dislocation core. Thus, the dislocation may be negatively or positively charged, and a field corresponding to the distributed charges along the dislocation loop should be superimposed to the present field. If there are free and removable charges in semiconductors, they may screen the piezoelectric polarization-induced charges, and the effective distance of the piezoelectric polarization may decrease. Also in the present work, we have assumed that the dislocation is located entirely within one material; otherwise, other kinds of dislocations, such as misfit dislocations, threading dislocations or dislocations piercing through interface, need to be considered.

ACKNOWLEDGMENTS

The work was supported by National Natural Science Foundation of China (Nos. 10872179, 11172273, and 11272052). The first author is also grateful for the support from China Scholarship Council.

APPENDIX: EXTENDED GREEN'S FUNCTIONS AND THEIR DERIVATIVES

The extended Green's function in piezoelectric bimaterials can be obtained using the 2D Fourier transform method in terms of the extended Stroh eigenrelation

$$[\mathbf{Q} + p(\mathbf{R} + \mathbf{R}^T) + p^2\mathbf{T}]\mathbf{a} = 0, \qquad (A1)$$

where $Q_{JK} = C_{iJKs}n_i n_s$, $R_{JK} = C_{iJK3}n_i$, $T_{JK} = C_{3JK3}$, $\mathbf{n} = [\cos\theta, \sin\theta, 0]^T$; p_i and $\boldsymbol{a}_i$ ($i=1\sim8$) are the eigenvalues and the associated eigenvectors, respectively; $\mathrm{Im}(p_i) > 0$, $p_{i+4} = \bar{p}_i$, $\mathbf{a}_{i+4} = \bar{\mathbf{a}}_i$ ($i=1\sim4$), $\mathbf{A} \equiv [\mathbf{a_1}, \mathbf{a_2}, \mathbf{a_3}, \mathbf{a_4}]$.

The extended Green's function tensor $\mathbf{G}$ at the field point $\boldsymbol{x}$ of a piezoelectric bimaterial due to a unit "point force" at $y_3 > 0$ is

$$\mathbf{G}(\mathbf{y};\mathbf{x}) = \begin{cases} \mathbf{G}^{\infty}(\mathbf{y};\mathbf{x}) + \mathbf{G}(\mathbf{y};\mathbf{x})^{Image}, & x_3 > 0 \\ \qquad\qquad + \mathbf{G}(\mathbf{y};\mathbf{x})^{Image}, & x_3 < 0 \end{cases}, \qquad (A2a)$$

$$\mathbf{G}(\mathbf{y};\mathbf{x})^{Image} = \begin{cases} \frac{1}{2\pi^2}\int_0^{\pi} \bar{\mathbf{A}}^{(1)}\mathbf{G}_u^{(1)}(\mathbf{A}^{(1)})^T \mathrm{d}\theta, & x_3 > 0 \\ \frac{1}{2\pi^2}\int_0^{\pi} \mathbf{A}^{(2)}\mathbf{G}_u^{(2)}(\mathbf{A}^{(1)})^T \mathrm{d}\theta, & x_3 < 0 \end{cases}, \tag{A2b}$$

with

$$(\mathbf{G}_u^{(1)})_{IJ} = \frac{(\mathbf{G}_1)_{IJ}}{-\mathbf{h}(\theta,\bar{p}_I^{(1)})\cdot\mathbf{x}+\mathbf{h}(\theta,p_J^{(1)})\cdot\mathbf{y}}, \quad (\mathbf{G}_u^{(2)})_{IJ} = \frac{(\mathrm{G}_2)_{IJ}}{-\mathbf{h}(\theta,p_I^{(2)})\cdot\mathbf{x}+\mathbf{h}(\theta,p_J^{(1)})\cdot\mathbf{y}}, \tag{A3a}$$

$$\mathbf{G}_1 = -(\bar{\mathbf{A}}^{(1)})^{-1}(\bar{\mathbf{M}}^{(1)}+\mathbf{M}^{(2)})^{-1}(\mathbf{M}^{(1)}-\mathbf{M}^{(2)})\mathbf{A}^{(1)}, \quad \mathbf{G}_2 = -(\mathbf{A}^{(2)})^{-1}(\bar{\mathbf{M}}^{(1)}+\mathbf{M}^{(2)})^{-1}(\mathbf{M}^{(1)}+\bar{\mathbf{M}}^{(1)})\mathbf{A}^{(1)}, \tag{A3b}$$

$$\mathbf{h}(\theta,p) = [\cos\theta,\sin\theta,p]^T, \quad \mathbf{M}^{(\alpha)} = -i\mathbf{B}^{(\alpha)}(\mathbf{A}^{(\alpha)})^{-1} \quad (\alpha = 1,\,2), \tag{A3c}$$

and $\mathbf{G}^{\infty}(\mathbf{y};\mathbf{x})$ the corresponding full-space Green's function tensor. The superscripts (1) and (2) denote, respectively, the quantities in Materials 1 and 2.

The derivatives of the extended Green's functions can be obtained as

$$\mathbf{G}(\mathbf{y};\mathbf{x})^{Image}_{,x_l\ldots y_p} = \begin{cases} \frac{1}{2\pi^2}\int_0^{\pi} \bar{\mathbf{A}}^{(1)}(\mathbf{G}_u^{(1)})_{,x_l\ldots y_p}(\mathbf{A}^{(1)})^T \mathrm{d}\theta, & x_3 > 0 \\ \frac{1}{2\pi^2}\int_0^{\pi} \mathbf{A}^{(2)}(\mathbf{G}_u^{(2)})_{,x_l\ldots y_p}(\mathbf{A}^{(1)})^T \mathrm{d}\theta, & x_3 < 0 \end{cases}, \tag{A4}$$

with

$$(\mathbf{G}_u^{(1)})_{IJ,x_l} = \frac{(\mathbf{G}_1)_{IJ}h_l(\theta,\bar{p}_I^{(1)})}{[-\mathbf{h}(\theta,\bar{p}_I^{(1)})\cdot\mathbf{x}+\mathbf{h}(\theta,p_J^{(1)})\cdot\mathbf{y}]^2}, \quad (\mathbf{G}_u^{(2)})_{IJ,x_l} = \frac{(\mathbf{G}_2)_{IJ}h_l(\theta,p_I^{(2)})}{[-\mathbf{h}(\theta,p_I^{(2)})\cdot\mathbf{x}+\mathbf{h}(\theta,p_J^{(1)})\cdot\mathbf{y}]^2}, \tag{A5a}$$

$$(\mathbf{G}_u^{(1)})_{IJ,x_ly_p} = \frac{-2(\mathbf{G}_1)_{IJ}h_l(\theta,\bar{p}_I^{(1)})h_p(\theta,p_J^{(1)})}{[-\mathbf{h}(\theta,\bar{p}_I^{(1)})\cdot\mathbf{x}+\mathbf{h}(\theta,p_J^{(1)})\cdot\mathbf{y}]^3}, \quad (\mathbf{G}_u^{(2)})_{IJ,x_ly_p} = \frac{-2(\mathbf{G}_2)_{IJ}h_l(\theta,p_I^{(2)})h_p(\theta,p_J^{(1)})}{[-\mathbf{h}(\theta,p_I^{(2)})\cdot\mathbf{x}+\mathbf{h}(\theta,p_J^{(1)})\cdot\mathbf{y}]^3}, \tag{A5b}$$

$$(\mathbf{G}_u^{(1)})_{IJ,x_ly_py_q} = \frac{6(\mathbf{G}_1)_{IJ}h_l(\theta,\bar{p}_I^{(1)})h_p(\theta,p_J^{(1)})h_q(\theta,p_J^{(1)})}{[-\mathbf{h}(\theta,\bar{p}_I^{(1)})\cdot\mathbf{x}+\mathbf{h}(\theta,p_J^{(1)})\cdot\mathbf{y}]^4}, \quad (\mathbf{G}_u^{(2)})_{IJ,x_ly_py_q} = \frac{6(\mathbf{G}_2)_{IJ}h_l(\theta,p_I^{(2)})h_p(\theta,p_J^{(1)})h_q(\theta,p_J^{(1)})}{[-\mathbf{h}(\theta,p_I^{(2)})\cdot\mathbf{x}+\mathbf{h}(\theta,p_J^{(1)})\cdot\mathbf{y}]^4}. \tag{A5c}$$

The extended Green's function tensor $\mathbf{G}$ at field point $\boldsymbol{x}$ due to a unit "point force" at $y_3 < 0$ is

$$\mathbf{G}(\mathbf{y};\mathbf{x}) = \begin{cases} +\,\mathbf{G}(\mathbf{y};\mathbf{x})^{Image}, & x_3 > 0 \\ \mathbf{G}^{\infty}(\mathbf{y};\mathbf{x}) + \mathbf{G}(\mathbf{y};\mathbf{x})^{Image}, & x_3 < 0 \end{cases}, \tag{A6a}$$

$$\mathbf{G}(\mathbf{y};\mathbf{x})^{Image} = \begin{cases} \frac{1}{2\pi^2}\int_0^{\pi} \bar{\mathbf{A}}^{(1)}\mathbf{G}_u^{(1)}(\bar{\mathbf{A}}^{(2)})^T \mathrm{d}\theta, & x_3 > 0 \\ \frac{1}{2\pi^2}\int_0^{\pi} \mathbf{A}^{(2)}\mathbf{G}_u^{(2)}(\bar{\mathbf{A}}^{(2)})^T \mathrm{d}\theta, & x_3 < 0, \end{cases} \tag{A6b}$$

where

$$(\mathbf{G}_u^{(1)})_{IJ} = \frac{(\mathbf{G}_1)_{IJ}}{-\mathbf{h}(\theta,\bar{p}_I^{(1)})\cdot\mathbf{x}+\mathbf{h}(\theta,\bar{p}_J^{(2)})\cdot\mathbf{y}}, \quad (\mathbf{G}_u^{(2)})_{IJ} = \frac{(\mathbf{G}_2)_{IJ}}{-\mathbf{h}(\theta,p_I^{(2)})\cdot\mathbf{x}+\mathbf{h}(\theta,\bar{p}_J^{(2)})\cdot\mathbf{y}}, \tag{A7a}$$

$$\mathbf{G}_1 = (\bar{\mathbf{A}}^{(1)})^{-1}(\bar{\mathbf{M}}^{(1)}+\mathbf{M}^{(2)})^{-1}(\bar{\mathbf{M}}^{(2)}+\mathbf{M}^{(2)})\bar{\mathbf{A}}^{(2)}, \quad \mathbf{G}_2 = -(\mathbf{A}^{(2)})^{-1}(\bar{\mathbf{M}}^{(1)}+\mathbf{M}^{(2)})^{-1}(\bar{\mathbf{M}}^{(1)}-\bar{\mathbf{M}}^{(2)})\bar{\mathbf{A}}^{(2)}. \tag{A7b}$$

The derivatives of the extended Green's functions for $y_3 < 0$ can be obtained similarly.

[1] I. B. Misirlioglu, S. P. Alpay, M. Aindow, and V. Nagarajan, Appl. Phys. Lett. **88**, 102906 (2006).
[2] D. Cherns and C. G. Jiao, Phys. Rev. Lett. **87**, 205504 (2001).
[3] J. Cai and F. A. Ponce, Phys. Status Solidi A **192**, 407 (2002).
[4] E. Müller, D. Gerthsen, P. Brückner, F. Scholz, Th. Gruber, and A. Waag, Phys. Rev. B **73**, 245316 (2006).
[5] D. Liu, M. Chelf, and K. W. White, Acta Mater. **54**, 4525 (2006).
[6] V. Nagarajan, C. L. Jia, H. Kohlstedt, R. Waser, I. B. Misirlioglu, S. P. Alpay, and R. Ramesh, Appl. Phys. Lett. **86**, 192910 (2005).
[7] Y. E. Pak, ASME J. Appl. Mech. **57**, 863 (1990).
[8] S. Minagawa, Int. J. Eng. Sci. **30**, 1459 (1992).
[9] J. X. Liu, S. Y. Du, and B. Wang, Mech. Res. Commun. **26**, 415 (1999).
[10] C. Shi, P. M. Asbeck, and E. T. Yu, Appl. Phys. Lett. **74**, 573 (1999).
[11] B. J. Chen, Z. M. Xiao, and K. M. Liew, Int. J. Eng. Sci. **42**, 1325 (2004).
[12] X. Wang and L. J. Sudak, Int. J. Solids Struct. **44**, 3344 (2007).
[13] K. Shintani, J. Appl. Phys. **69**, 8119 (1991).
[14] N. G. Weimann, L. F. Eastman, D. Doppalapudi, H. M. Ng, and T. D. Moustakas, J. Appl. Phys. **83**, 3656 (1998).
[15] D. C. Look and J. R. Sizelove, Phys. Rev. Lett. **82**, 1237 (1999).
[16] D. Jena, A. Gossard, and U. K. Mishra, Appl. Phys. Lett. **76**, 1707 (2000).
[17] X. Xu, X. Liu, S. Yang, J. Liu, H. W. Q. Zhu, and Z. Wang, Appl. Phys. Lett. **94**, 112102 (2009).
[18] G. Liu, J. Wu, G. Zhao, S. Liu, W. Mao *et al.*, Appl. Phys. Lett. **100**, 082101 (2012).
[19] S. Minagawa and K. Shintani, Philos. Mag. A **51**, 277 (1985).
[20] S. Shintani and S. Minagawa, Philos. Mag. A **62**, 275 (1990).
[21] S. Minagawa, Mech. Mater. **35**, 453 (2003).
[22] J. P. Nowacki and V. I. Alshits, *Dislocations in Solids* (Elsevier B.V., 2007).
[23] D. M. Barnett and J. Lothe, Phys. Status Solidi B **67**, 105 (1975).
[24] E. Pan and F. Tonon, Int. J. Solids Struct. **37**, 943 (2000).
[25] X. Han and E. Pan, "Fields produced by three-dimensional dislocation loops in anisotropic magneto-electro-elastic materials," Mech. Mater. (in press).
[26] E. Pan and F. G. Yuan, Int. J. Eng. Sci. **38**, 1939 (2000).
[27] H. Morkoc and J. Leach, *Polarization Effects in Semiconductors From Ab Initio Theory to Device Applications* (Springer, 2007).
[28] O. Ambacher, B. Foutz, J. Smart, J. R. Shealy, N. G. Weimann *et al.*, J. Appl. Phys. **87**, 334 (2000).
[29] O. Ambacher, J. Smart, J. R. Shealy, N. G. Weimann, K. Chu *et al.*, J. Appl. Phys. **85**, 3222 (1999).